Pervasive interactions between methyl torsion and low frequency vibrations in S_0 and S_1 *p*-fluorotoluene

Jason R. Gascooke (iD), Laurence D. Stewart, Paul G. Sibley, and Warren D. Lawrance (iD)

View Online   Export Citation   CrossMark

ARTICLES YOU MAY BE INTERESTED IN

AIP Publishing

Pervasive interactions between methyl torsion and low frequency vibrations in S_0 and S_1 *p*-fluorotoluene

Jason R. Gascooke, Laurence D. Stewart, Paul G. Sibley,[a)] and Warren D. Lawrance[b)]
College of Science and Engineering, Flinders University, G.P.O. Box 2100, Adelaide, SA 5001, Australia

We report two dimensional laser induced fluorescence spectral images exploring the lower torsion-vibration manifolds in S_0 ($E < 560$ cm^{-1}) and S_1 ($E < 420$ cm^{-1}) *p*-fluorotoluene. Analysis of the images reveals strong torsion-vibration interactions and provides an extensive set of torsion-vibration state energies in both electronic states (estimated uncertainty ±0.2 cm^{-1}), which are fit to determine key constants including barrier heights, torsional constants, and torsion-vibration interaction constants. The dominant interactions in both electronic states are between methyl torsion (internal rotation) and the lowest frequency out-of-plane modes, D_{20} and D_{19}, both of which involve a methyl wagging motion. This is the second aromatic (following toluene) for which a significant interaction between torsion and methyl out-of-plane wagging vibrations has been quantified. Given the generic nature of this motion in substituted toluenes and similar molecules, this mechanism for torsion-vibration coupling may be common in these types of molecules. The inclusion of torsion-vibration coupling affects key molecular constants such as barrier heights and torsional (and rotational) constants, and the possibility of such an interaction should thus be considered in spectral analyses when determining parameters in these types of molecules. *p*-Fluorotoluene is the first molecule in which the role of methyl torsion in promoting intramolecular vibrational energy redistribution (IVR) was established and the observed torsion-vibration coupling provides one conduit for the state mixing that is a precursor to IVR, as originally proposed by Moss *et al.* [J. Chem. Phys. **86**, 51 (1987)]. *Published by AIP Publishing.* https://doi.org/10.1063/1.5035461

I. INTRODUCTION

Internal rotation is a textbook example of a large amplitude motion, with methyl rotation having received particular attention.[1] Methyl group rotation was originally regarded as being barrierless, but Kemp and Pitzer's analysis of thermodynamic data for ethane revealed the presence of a sizable, ~1000 cm^{-1}, barrier in that molecule,[2] the origin of which continues to be debated.[3–5] Since the 1950s, spectroscopic techniques, particularly microwave spectroscopy, have provided detailed insights into methyl torsion. The theoretical foundations for spectral analysis were developed during the 1950s and 1960s and underpin the computer codes used today.[6–8] The problem is considered in terms of the interaction of internal rotation of the methyl group with overall rotation of the molecule,[6,9] with the *methyl rotation assumed to be independent of the molecular vibrations*, at least for the lower torsional states.[1,9–11] Observed rotational line positions are routinely fit with a precision of ~1 part in 10^8 (Refs. 6 and 9), which provides compelling evidence for the validity of the underlying assumptions. The parameters extracted from spectral analysis provide insights such as the magnitude of the barrier to torsional motion and, through the rotational constants,

the molecule's geometry. These can be compared with the results of *ab initio* calculations and hence provide a test of their accuracy.

We have recently shown, however, that this approach is unsound in toluene as the methyl torsional motion is strongly influenced by a low frequency, out-of-plane "methyl wag" vibration.[12–14] Exploiting the technique of two dimensional laser induced fluorescence (2D-LIF),[15] we determined torsion and torsion-vibration energies in both the S_0 and S_1 electronic states and showed that they were perturbed, with accompanying changes in the rotational contours. It was further demonstrated that toluene rotational line data can be successfully fitted within the torsion-vibration interaction model so that the results from electronic spectroscopy and rotational spectroscopy can be successfully explained using the same model.[12–14] In performing this analysis, it was demonstrated that rotational line data can be insensitive to torsion-vibration interactions, which explains why the toluene data were successfully analyzed previously without it being included.[12] However, the torsion-vibration interactions conspire to alter fundamental constants including F, the rotational constant associated with methyl rotation, and V_6, the torsional barrier height.[12] Given the generic nature of the methyl wagging motion that gives rise to the interactions seen for toluene, there is a potential implication for spectral analyses of substituted toluenes more generally. This leads to the key question of whether the form of torsion-vibration interaction seen in toluene is present in other molecular systems. This has implications for the reliability

---

a)Present address: Centre for Gravitational Physics, Department of Quantum Science, Research School of Physics and Engineering, Australian National University, 2601, Canberra, Australia.
b)Author to whom correspondence should be addressed: warren.lawrance@flinders.edu.au

of methyl geometries and barriers implied by the constants determined for these types of molecules using conventional assumptions.

In this context, we have undertaken a detailed study and analysis of torsion and torsion-vibration states in the low energy regions of S_0 and S_1 *p*-fluorotoluene (*p*FT) where the out-of-plane and in-plane methyl wagging modes are found. *p*FT is the simplest substituted toluene that retains the G_{12} symmetry of the parent. Interestingly, it has played a role in studies of intramolecular vibrational energy redistribution (IVR) and it is now over 30 years since it was first demonstrated by comparing *p*FT and *p*-difluorobenzene that the onset of IVR is enhanced by the presence of a methyl rotor,[16–21] giving a strong indication that there is interaction between the torsional and vibrational motions.

Wright's group has recently examined the spectroscopy of toluene[22,23] and the substituted toluenes *p*-xylene[24,25] and *p*FT.[26–28] Using zero electron kinetic energy (ZEKE) spectroscopy, they examined the first excited singlet electronic state, S_1, of *p*FT and the ground electronic state, D_0^+, of its cation, revising a number of the S_1 assignments. Earlier assignments of the *p*FT S_0-S_1 spectrum were based on two key studies that used laser induced fluorescence (LIF) in combination with dispersed fluorescence (DF) spectroscopy.[29,30] Spectral features had been assigned to torsional modes up to $m = 8$ and fits to these torsional levels yielded values for the torsional barrier heights, V_6, and torsional rotation constants, F, in S_0 and S_1. However, with Gardner *et al.* revising a number of these assignments,[26] particularly those involving high m, the values determined for these constants are doubtful. The dispersed fluorescence studies of S_0 have been of modest resolution compared with the laser-excited S_1 studies, and the few published spectra lack the precision required to probe for the effects of any interaction of torsion with methyl wagging vibrations.

In the present paper, we explore the interaction between torsion and low frequency vibrations in S_0 and S_1 *p*FT through the use of 2D-LIF. Specifically, we address the question of whether a coupling between the torsional motion and the out-of-plane methyl wag vibrational mode D_{20}, as observed for both S_0 and S_1 toluene, is also present in S_0 and S_1 *p*FT. Furthermore, we consider the extent to which other low frequency methyl "wagging" modes are involved in such interactions. This issue is important given the assumption underpinning analyses of rotational spectra that the methyl and low amplitude vibrations are separable.[31] Additionally, this study provides insight into the coupling between methyl rotation and low frequency vibrations that classical Hamiltonian modeling has suggested plays a role in the enhancement of IVR by the methyl rotor.[32]

The interaction between torsion and low frequency vibrations is revealed through both strong local perturbations and long-range interactions that result in subtle shifts in band positions. Consequently, a comprehensive analysis of all bands observed is required in order to produce a reliable database of observed frequencies, with the modeling requiring band positions to higher precision than has previously been reported. Given our focus on interactions between methyl torsion and vibrations involving methyl wagging, we have examined the

lowest 560 cm^{-1} of the S_0 state and lowest 420 cm^{-1} of the S_1 state. Frequency changes on electronic excitation mean that these two regions largely cover the same set of states. It will be shown that torsion-vibration interactions are pervasive in these regions. Detailed modeling of the S_1 and S_0 energies reveals extensive interactions between low frequency vibrations and methyl torsion.

II. EXPERIMENTAL DETAILS

The experimental setup for 2D-LIF has been presented previously and the reader is referred to Ref. [33] for details. Laser-induced fluorescence (LIF) or dispersed fluorescence spectra are obtained by integrating the 2D images over the emission or excitation wavelengths, respectively. Importantly, the relative intensities of bands in the "LIF" spectrum extracted from an image depend on the particular emission bands present in the spectral window monitored (see, for example, Ref. [34]): the "LIF" spectrum will only show bands when the state that has been excited emits in the spectral window being monitored. Further details of the 2D-LIF imaging technique are given in Ref. [15].

III. BACKGROUND

A. Methyl rotation and the observed torsional bands

*p*FT is an example of a methyl rotor attached to a frame with C_{2v} point group symmetry, and consequently, there is a 6-fold barrier to methyl rotation, with the barrier height denoted by V_6. *p*FT belongs to the G_{12} molecular symmetry group, the same as toluene. Previous studies have determined S_0 and S_1 barriers that are quite low, 4.8 cm^{-1} [35,36] and ~ -33 cm^{-1},[29,30] respectively. The modelling and spectroscopy for methyl torsional states in a molecule with G_{12} symmetry have been summarised in our previous studies of toluene.[12–14,37] In brief, the energies of this slightly hindered rotor are calculated as the eigenvalues of the Hamiltonian matrix constructed in the basis of free rotor states, $\psi = \frac{1}{\sqrt{2\pi}} \exp(i\underline{m}\alpha)$, where α is the torsional angle and $\underline{m}$ is the torsional angular momentum quantum number, which takes values of 0, ±1, ±2, ...[37–40] The non-zero Hamiltonian matrix elements are

$$H_{\underline{m},\underline{m}} = \underline{m}^2 \left(F + \underline{m}^2 F_{\underline{m}} \right) + \frac{V_6}{2} \tag{1}$$

and

$$H_{\underline{m},\underline{m}\pm 6} = -\frac{V_6}{4}, \tag{2}$$

where F is the constant for internal rotation for $\underline{m} = 0$ and F_m is effectively a centrifugal distortion term,[41] which has also been labeled dF.[42] This latter term is usually ignored in fits to torsional band positions. For *p*FT, the off-diagonal terms are small and the hindered methyl rotor states are generally little perturbed from the free rotor states. They are labeled by m, where $m = |\underline{m}|$. For example, the perturbed $\underline{m} = \pm 1, \pm 2, \pm 4, \ldots$ states remain degenerate and are denoted $m = 1, 2, 4, \ldots$ and, where the G_{12} molecular symmetry is included, are identified as $1e''$, etc. However, for the degenerate $\underline{m} = \pm 3n$ ($n = 1, 2, \ldots$) pairs, one obtains symmetric and

anti-symmetric linear combinations of the $\underline{m} = -3n$ and $+3n$ components. We use $3n(+)$ to indicate the symmetric combination and $3n(-)$ the anti-symmetric one. This description of the torsional states ignores the interaction of torsion and vibration but provides an appropriate starting point for discussion of the spectra.

The methyl torsional levels and transitions are labeled using the usual spectroscopic convention: m_a denotes the state with $m = a$ in S_0, m^b denotes the state with $m = b$ in S_1, and m_a^b denotes a transition between them. The $m = 3n$ and $m = 3n \pm 1$ states ($n = 0, 1, 2, \ldots$) belong to different nuclear spin states,[42,43] and with supersonic cooling, the initial m state population collapses to be almost entirely in $m = 0$ and $m = 1$, which have almost equal population.[44] The Δm changes seen in the spectra and their relative intensities are understood in terms of a rapidly converging trigonometric expansion of the transition dipole in terms of the torsion angle,[37,44]

$$M(\alpha) = M_0 + M_3 \cos(3\alpha) + M_3' \sin(3\alpha) + M_6 \cos(6\alpha)$$
$$+ M_6' \sin(6\alpha) + \cdots , \qquad (3)$$

where $M(\alpha)$ is the transition dipole. When the S_0 and S_1 torsional barriers are low as they are for pFT, the dominant transitions are those involving $\Delta m = 0$. The $\Delta m = \pm 3$ transitions, m_1^2, $m_0^{3(+)}$, and m_1^4, are typically a few percent of the $\Delta m = 0$ transitions and are induced through the M_3 term, while the $\Delta m = \pm 6$ transitions, m_1^5, $m_0^{6(+)}$, and m_1^7, are generally much weaker again and derive their intensity from both the M_6/M_6' terms and the M_0 term. {The M_0 Franck-Condon components of the m_1^5, $m_0^{6(+)}$, and m_1^7 transitions arise from the $-V_6/4$ term mixing free rotor states separated by $\Delta \underline{m} = \pm 6$ [see Eq. (2)].} The $m_0^{3(-)}$ transition is forbidden by these terms but gains intensity through torsion-rotation coupling, which leads to its relative intensity being temperature dependent.[37]

B. Vibrational mode numbering scheme

Several mode numbering schemes have been used for the pFT vibrations. To bring order to the numbering in *para*-disubstituted benzenes, Andrejeva *et al.* presented a systematic vibrational numbering scheme based on *p*-diflurobenzene as the template and an analysis of how the vibrational motions change with substituent mass.[45] Their notation was used by Gardner *et al.*[26] in their revision of $S_1 \leftarrow S_0$ assignments and is adopted here. The currently accepted S_0 frequencies in this notation are provided in Table 1 of Ref. 26.

IV. EXPERIMENTAL RESULTS

Figure 1 shows the 2D-LIF spectral image equivalent of a dispersed fluorescence scan from the 0^0 level as a probe of S_0 states. It shows fluorescence in the region 0_0^0 to $0_0^0 - 560$ cm^{-1} with the laser excitation scanned across the 0_0^0 band, which encompasses the overlapped m_0^0 and m_1^1 transitions. With fluorescence collected in spectral segments ~90 cm^{-1} wide, the figure is composed of multiple images stitched together.

Figure 2 shows a 2D-LIF spectral image of the lowest 420 cm^{-1} of the $S_1 \leftarrow S_0$ excitation spectrum, with the spectrometer set to detect emission between ~36 860 and ~36 780 cm^{-1}, which is a window incorporating the 0_0^0 band and an ~80 cm^{-1} region to lower energy. While many of the absorption features have emission bands in this region, it does not allow observation of vibrational modes with a significant frequency change between S_0 and S_1, specifically D_{14} and D_{19}. The D_{19} torsional bands were explored through a separate scan with the spectrometer positioned to monitor the $19_1^1 m_n^n$ bands, and this region has been added to the image in Fig. 2 with appropriate intensity scaling. D_{14} is expected to show a large 205 cm^{-1} red shift in the fluorescence axis in 2D-LIF images, given the reported S_0 and S_1 frequencies of 404 and 199 cm^{-1}, respectively.[18,26] D_{14} and its combinations and overtones were explored in a further set of experiments, and the relevant 2D-LIF images and extracted spectra are provided in the supplementary material. The absorption transitions associated with methyl torsion are generally observed via the $\Delta m = 0$ fluorescence transition since this is by far the strongest band, as discussed in Sec. III. The assignments, which are discussed in detail in
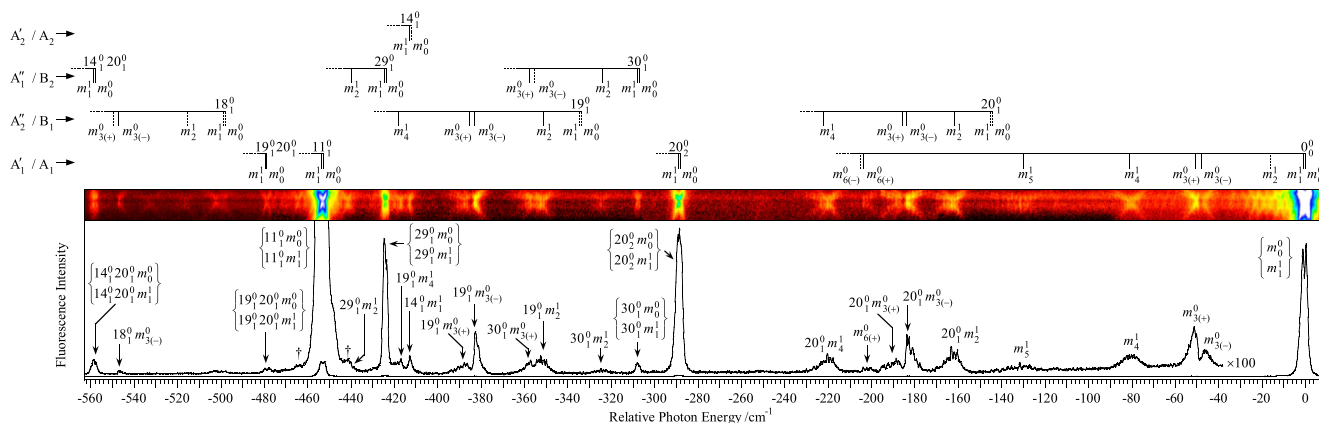
FIG. 1. The 2D-LIF spectral image of the pFT emission spectrum from 0_0^0 to $0_0^0 - 560$ cm^{-1}, with laser excitation scanning a 5.3 cm^{-1} region about the 0_0^0 band at 36 860.0 cm^{-1}. A vertical integration of the spectral image, which corresponds to the 0^0 fluorescence spectrum, is shown below the image. Assignments of the features are shown on the spectrum and reported in Table I. Peaks arising from grating ghosts are marked with a † symbol. The torsional combs for each vibration are shown above the image, with observed features indicated by solid lines.

FIG. 2. (a) A 2D-LIF spectral image associated with the first ~420 cm^{-1} of the pFT S$_1$ ← S$_0$ excitation spectrum. The scan was collected in several sections and intensities matched for overlapped features. Unlabeled features are associated with pFT-Ar$_n$ van der Waals complexes. A separate sc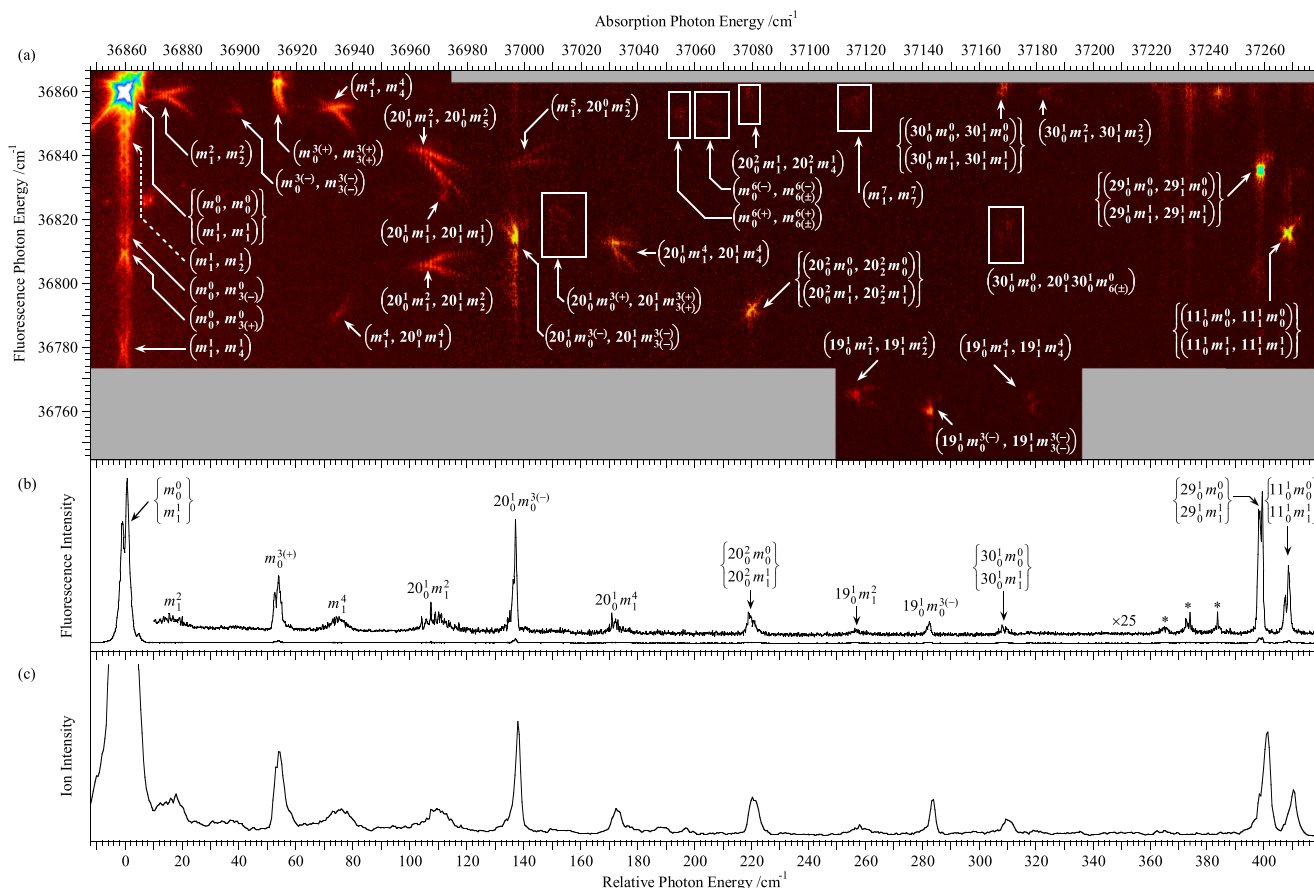an monitoring the D_{19} torsional levels is appended to the main image. (b) The "LIF" spectrum extracted by vertically integrating the image. Asterisks indicate features associated with pFT-Ar$_n$ van der Waals complexes. (c) A REMPI spectrum of this region, provided by Wright and co-workers.[26]

the supplementary material, are shown on the images in Figs. 1 and 2. The unassigned features in Fig. 2 arise from van der Waals complexes.

The S$_0$ and S$_1$ energies of the torsion-vibration states observed are determined by extracting the band origins from the features observed. In many cases, the same terminating state in S$_0$ is revealed through multiple 2D-LIF features, which provides a check for the consistency and accuracy of the values determined. The rotational contours for torsional bands are often broad, making it difficult to determine accurate values for the band origins in the absence of fitting the contours. The broad contours arise due to torsion-rotation coupling, which leads to a large K_a band head spacing.[37,42] As we have demonstrated previously, the most accurate determination of band origins comes from comparing experimental and calculated rotational contours,[13,14] and this method has been used in the present work. As discussed in detail in Refs. 13 and 14, the final values for the band origins are determined using an iterative process where torsion-vibration couplings are introduced as required to reproduce the contours. For the pFT analysis, the 2D contours were fit directly rather than using the 1D absorption and fluorescence projections as was done previously.[13,14] Separate, high signal images were collected for the weaker features in Fig. 2 for this purpose. Table I lists the S$_0$ and S$_1$ energies for the states observed; based on multiple

observations of the same state, they are estimated to be accurate to ±0.2 cm^{-1}.

As noted in the Introduction, a comprehensive analysis of all bands observed is required to produce a reliable database of observed torsion-vibration transition frequencies, as this forms the basis for the experimental torsion-vibration state energies that underpin the modeling of torsion-vibration interactions. As this analysis is quite detailed, we here provide three exemplars to illustrate how the torsion-vibration interactions are observed in the images. The complete analysis is provided in the supplementary material.

A. Exemplar 1: Perturbations to D_{20} and its torsional states in S$_0$ observed via emission from 0^0

Previous authors have most commonly assigned the lowest S$_0$ vibrational mode, D_{20}, a frequency of 157 cm^{-1}, the value reported for the liquid,[46] but Andrejeva *et al.* have noted that this value is surprisingly far from the computed value of 141 cm^{-1}.[45] Okuyama *et al.*[29] assigned the D_{20} frequency as 180 cm^{-1} (ν_{11} in their notation) from their gas phase dispersed fluorescence spectra, but Gardner *et al.*[26] have reassigned the corresponding absorption feature to a torsional level in combination with D_{20}, with which we concur (see Sec. IV B and the supplementary material). Gas phase thermodynamic calculations require $D_{20} = 144$ cm^{-1} for agreement between the

TABLE I. The S_0 and S_1 torsion-vibration state relative energies, listed in ascending order, determined by analysis of the 2D-LIF spectral images.

	S_0		S_1
Level	Relative energy[a]	Level	Relative energy[a]
m_1	0	m^1	0.0
m_0	0	m^0	0.0
m_2	−16.3	m^2	15.3
$m_{3(−)}$	−48.1	$m^{3(−)}$	40.7
$m_{3(+)}$	−50.4	$m^{3(+)}$	53.1
m_4	−81.6	m^4	75.8
m_5	−129.6	$20^1 m^2$	108.1
$20_1 m_1$	−144.4	$20^1 m^1$	112.1
$20_1 m_2$	−162.0	$20^1 m^{3(−)}$	137.0
$20_1 m_{3(−)}$	−183.9	m^5	141.0
$20_1 m_{3(+)}$	−186.0	$20^1 m^{3(+)}$	150.1
$m_{6(+)}$	−204.1	$20^1 m^4$	173.1
$m_{6(−)}$	−205.3	$m^{6(+)}$	196.6
$20_1 m_4$	−221.7	$14^1 m^1$	197.8
m_7	−265.8	$m^{6(−)}$	201.4
$20_2 m_0$	−288.3	$20^2 m^1$	219.5
$20_2 m_1$	−288.9	$20^2 m^0$	220.1
$30_1 m_0$	−307.6	$19^1 m^2$	256.8
$30_1 m_1$	−307.6	m^7	262.4
$30_1 m_2$	−324.0	$19^1 m^{3(−)}$	282.4
$19_1 m_2$	−351.6	$14^1 20^1$	310.2
$20_1 m_{6(+)}$	−349.9	$30^1 m^1$	309.4
$20_1 m_{6(−)}$	−351.6	$30^1 m^0$	310.7
$30_1 m_{3(−)}$	−355.5	$19^1 m^4$	319.8
$30_1 m_{3(+)}$	−357.4	$30^1 m^2$	324.1
$19_1 m_{3(−)}$	−383.2	$30^1 m^{3(−)}$	349.7
$19_1 m_{3(+)}$	−385.6	$19^1 20^1 m^0$	351.7
$30_1 m_4$	−389.1	$19^1 20^1 m^1$	. . .
$19_1 m_4$	−418.1	$30^1 m^{3(+)}$	361.3
$14_1 m_1$	−413.2	$30^1 m^4$	384.8
29_1	−423.9	$14^2 m^0$	396.9
11_1	−452.8	$14^2 m^1$	397.5
$19_1 20_1 m_0$	−479.1	29^1	399.0
$19_1 20_1 m_1$	−479.2	11^1	408.1
$18_1 m_{3(−)}$	−547.9	$19^2 m^0$	480.3
$14_1 20_1 m_0$	−557.9	$19^2 m^1$	482.9
$14_1 20_1 m_1$	−559.1		
$14_1 20_1 m_{3(+)}$	−599.6		
$14_1 m_{6(−)}$	−618.8		
28_1	−639.9		
$14_2 m_1$	−822.8		
$14_2 m_0$	−823.5		
9_1	−842.9		
29_2	−849.5		
$11_1 29_1$	−876.7		
$19_2 m_0$	−670.0		
$19_2 m_1$	−670.0		

[a]Energies are relative to $m = 0$ for states involving m values of 0, 3(−), 3(+), 6(−), and 6(+) and $m = 1$ for states involving m values of 1, 2, 4, 5, and 7. This references their energies to the appropriate nuclear spin isomer. $m = 0$ and $m = 1$ belong to different nuclear spin isomers, and their separation cannot be determined from the spectra.

observed and calculated entropy,[47] a value much closer to the computational prediction.[45] Gardner *et al.* assigned the S_1 D_{20} frequency to be 110 cm^{-1}, and given the D_{20} sequence band separation of −34.5 cm^{-1},[48] this requires an S_0 D_{20} frequency of ∼145 cm^{-1}.

20_1^0 is symmetry forbidden and the selection rules indicate that the strongest bands from 0^0 will be those involving $\Delta\underline{m} = \pm 3$: $20_1^0 m_2^1$, $20_1^0 m_{3(−)}^0$, $20_1^0 m_{3(+)}^0$, and $20_1^0 m_4^1$. These D_{20} torsional transitions are seen but their relative positions indicate that the states are perturbed by a torsion-specific interaction as follows. $20_1^0 m_2^1$ is observed at $m_1^1 − 162.0$ cm^{-1}, $20_1^0 m_{3(−)}^0$ at $m_0^0 − 183.9$ cm^{-1}, $20_1^0 m_{3(+)}^0$ at $m_0^0 − 186.0$ cm^{-1}, and $20_1^0 m_4^1$ at $m_1^1 − 221.7$ cm^{-1}. Using the $m_{3(−)}^0$, $m_{3(+)}^0$, and m_4^1 transition energies, the S_0 D_{20} frequency can in principle be determined but this yields different values of 135.8, 135.6, and 140.1 cm^{-1}, respectively. There is a significant difference of ∼4.4 cm^{-1} when using the $m_{3(\pm)}^0$ versus m_4^1 transitions. Furthermore, the m_1-m_2 separation of 16.3 cm^{-1} determined from the spectral features in Fig. 2 (see the supplementary material) indicates a different value again of $D_{20} = 145.7$ cm^{-1}. *It is clear that the torsional states of 20_1 have different energies compared with those of 0_0*, which is a signature of torsion-vibration coupling.[13,14] The rotational structure of the $(20_0^1 m_0^{3(−)}, 20_1^1 m^{3(−)})$ feature (Fig. 2) reveals perturbations in the terminating S_0 states, providing direct evidence for torsion-vibration coupling involving D_{20} in S_0, as discussed in Sec. IV B.

B. Exemplar 2: Interaction between D_{20} and torsional states in S_1

Figure 2 shows that there is significant spectral complexity starting in the region above $0_0^0 + 100$ cm^{-1}. The complexity is associated with the introduction of torsional bands associated with D_{20} that couple with those of 0^0. D_{20} has a_2'' symmetry and one quantum changes in this mode must be accompanied by $\Delta\underline{m} = \pm(6n + 3)$ (where n is an integer: 0, 1, . . .) changes in the free rotor quantum number.

The broad absorption feature centred near $0_0^0 + 108$ cm^{-1} appears at a lower energy than expected for m_1^5, and the image shows emission from this band terminating in both m_5 and $20_1 m_2$. These emission features have the same absorption profile, showing that they arise from a single absorption band and not two overlapped bands and revealing that the emitting level is a mixture of m^5 and $20^1 m^2$. The band terminating in $20_1 m_2$ has 14% more intensity than that terminating in m_5, indicating that the emitting state has slightly more $20^1 m^2$ than m^5 character. On this basis, the absorption feature is labeled $20_0^1 m_1^2$ to recognise the slightly larger component, consistent with the assignment of Gardner *et al.*[26] Rotational contour analysis gives a value of $m_1^1 + 108.1$ cm^{-1} for the band origin compared with a value of 112 cm^{-1} estimated by Gardner *et al.*, highlighting the difficulty of identifying band origins for perturbed torsional bands when extended rotational contours occur.

The feature at $0_0^0 + 137.0$ cm^{-1} is quite unusual, being sharp in absorption but extending over a considerable range in emission. It was assigned to 20_0^1 (in the mode numbering scheme used here) by Okuyama *et al.*;[29] however, Gardner *et al.* reassigned it as $20_0^1 m_0^{3(−)}$. With this revised assignment, an accompanying, weak $20_0^1 m_0^{3(+)}$ feature is expected to higher energy and this is indeed observed at $0_0^0 + 150.1$ cm^{-1}. A higher signal scan recorded over this region
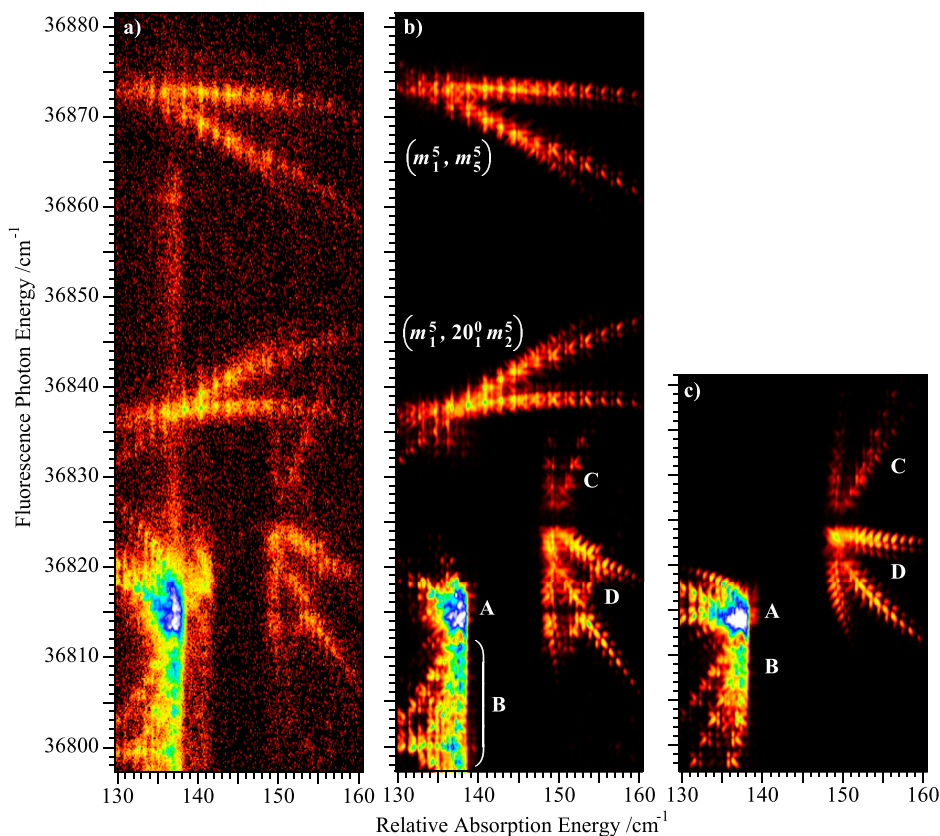
FIG. 3. (a) A higher signal 2D-LIF image recorded over the $0^0_0 + 130$ cm^{-1} to $0^0_0 + 160$ cm^{-1} region, which encompasses the $20^1_0 m^{3(-)}_0$, m^5_1, and $20^1_0 m^{3(+)}_0$ absorption transitions. (b) The 2D-LIF image predicted using the parameters derived from the S_0 and S_1 fits with V_6 varied (Table V; see the text). (c) The 2D-LIF image expected in the absence of torsion-vibration coupling. The indicated features are (A) $(20^1_0 m^{3(-)}_0,\ 20^1_1 m^{3(-)}_{3(-)})$, (B) $(20^1_0 m^{3(-)}_0,\ 20^1_1 m^{3(-)}_{3(+)})$, (C) $(20^1_0 m^{3(+)}_0,\ 20^1_1 m^{3(+)}_{3(-)})$, and (D) $(20^1_0 m^{3(+)}_0,\ 20^1_1 m^{3(+)}_{3(+)})$.

confirms the assignment through the rotational structure (Fig. 3). The rotational structure reveals perturbations in the terminating S_0 states, providing direct evidence for torsion-vibration coupling in S_0. Our ability to model these 2D rotational contours on the basis of torsion-vibration coupling is discussed in Sec. V C.

Slightly overlapped with $20^1_0 m^{3(-)}_0$ in absorption but extending to higher energy is the second of the $20^1 m^2/m^5$ torsion-vibration coupled pair, which we label m^5, with the caveat as before that the two zero order states are significantly mixed. Gardner *et al.* reported the absorption at $0^0_0 + 142$ cm^{-1}.[26] The feature seen terminates in $20_1 m_2$. This assignment requires that there is a second emission band, terminating in m_5, and a scan over the appropriate region confirms its presence (see Fig. 3).

It is clear from analysis of the image in Fig. 2 that there is a significant torsion-vibration interaction in S_1 involving D_{20}.

C. Exemplar 3: Interaction between D_{19} and torsional states in S_1

With D_{19} having a significant frequency change between S_0 and S_1, the absorption transitions to the torsional states of D_{19} are readily assigned from the features seen in the 2D-LIF image of Fig. 2: $19^1_0 m^2_1$ occurs at $m^1_1 + 256.8$ cm^{-1}, $19^1_0 m^{3(-)}_0$ occurs at $m^0_0 + 282.4$ cm^{-1}, and $19^1_0 m^4_1$ occurs at $0^0_0 + 319.8$ cm^{-1}. These are consistent with the assignments of Gardner *et al.*[26] Similar to the D_{20} situation, the presence of a torsion-vibration interaction involving D_{19} is revealed by changes in the torsional band separations. Using the

$19^1_0 m^{3(-)}_0$ and $m^{3(-)}_0$ band positions gives an S_1 D_{19} frequency of 241.7 cm^{-1}, while using $19^1_0 m^4_1$ and m^4_1 gives 244.0 cm^{-1}, a 2.3 cm^{-1} difference. Gardner *et al.* noted that $19^1_0 m^4_1$ occurred at higher energy than expected and postulated an interaction between m^7 and $19^1 m^4$.[26]

The involvement of D_{19} in torsion-vibration coupling is further illustrated by perturbations in the m^7_1 and $19^1_0 m^2_1$ rotational contours (see the supplementary material). Both contours show the effects of coupling between the almost isoenergetic m^7 and $19^1 m^2$ states. Although superficially this appears to involve a near-resonant $\Delta m = 9$ coupling, the modeling to be discussed in Sec. V indicates that it occurs via the indirect pathway $m^7 \leftrightarrow 20^1 m^4 \leftrightarrow 19^1 20^1 m^1 \leftrightarrow 19^1 m^2$. This involves strong first order $\Delta v = \pm 1$, $\Delta \underline{m} = \pm 3$ couplings at each step that combine to produce the weak, near-resonant interaction observed.

D. Summary of torsion-vibration interactions observed

As illustrated by the examples above and discussed in detail in the supplementary material, a number of torsion-vibration interactions have been identified from the analysis of the spectral features observed. These interactions are summarised in Table II. A number of second order interactions are revealed through local perturbations, while first order torsion-vibration coupling is clearly evident through either major perturbations or shifts in the torsional level spacing for that mode. It is clear from the spectral analysis that torsion-vibration couplings are significant in the low energy regions of both S_0 and S_1 pFT. The modeling of these interactions is discussed in Sec. V.

TABLE II. Torsion-vibration interactions in S_0 and S_1 pFT identified through analysis of the 2D-LIF images.

Coupling operator[a]	Evidence
Ground electronic state, S_0	
$q_{20}\sin(3\alpha)$	(i) Different spacings for the torsional levels of 20_1 versus 0_0; (ii) Perturbations in the 2D rotational contours, especially for the terminating level $20_1 m_{3(-)}$; (iii) Increased separation between $20_2^0 m_0^0$ and $20_2^0 m_1^1$ compared with m_0^0 and m_1^1
$q_{14} q_{19}\cos(3\alpha)$	Interaction between $14_1 m_1$ and $19_1 m_4$
Excited electronic state, S_1	
$q_{20}\sin(3\alpha)$	(i) Strong, near resonant coupling between m^5 and $20^1 m^2$; (ii) Significant shifts in the torsional energies for 20^1 compared with 0^0; (iii) Perturbations in the 2D rotational contours, particularly those involving the m states of 20^1
$q_{19}\sin(3\alpha)$	(i) Different spacings for the torsional levels of 19^1 versus 0^0; (ii) Interaction between $19^1 m^2$ and m^7 (see the text for coupling pathways)
$q_{30}\cos(3\alpha)$	Slightly reduced $3(-)$-$3(+)$ separation for 30^1 compared with 0^0
$q_{14}\sin(6\alpha)$	(i) An interaction between $14^1 m^0$ and $m^{6(-)}$ is required to explain the $m_0^{6(-)}$ rotational contour; (ii) The interaction between 14^2 and $14^1 m^{6(-)}$ is observed through emission to $14_1 m_{6(-)}$
$q_{14} q_{19}\cos(3\alpha)$	Perturbation of $19^2 m^0$ by $14^1 19^1 m^{3(+)}$
$q_{20} q_{30}\sin(6\alpha)$	Interaction between $30^1 m^0$ and $20^1 m^{6(-)}$ observed through emission to $20_1 m_{6(-)}$

[a]The coupling terms are defined and discussed in Sec. V (see also Table III).

V. GLOBAL MODELING OF THE TORSION AND TORSION-VIBRATION STATE ENERGIES

The spectral analysis has revealed that torsion-vibration couplings permeate the low energy regions of both S_0 and S_1 pFT. Modeling these interactions provides crucial insights into the magnitude of the interactions and their extent. It also provides unperturbed values for the constants relating to the torsional motion: F, the internal rotation constant, and V_6, the torsional barrier height.

The treatment of methyl rotation/torsion has been discussed in Sec. III, with the Hamiltonian matrix elements in the free rotor basis being given in Eqs. (1) and (2). Depending on the vibrational symmetry, torsion-vibration coupling involves terms of the form[17,34,49]

$$k_{ij\ldots k}^{T-V}q_i q_j \cdots q_k\cos(3n\alpha) \quad \text{or} \quad k_{ij\ldots k}^{T-V}q_i q_j \cdots q_k\sin(3n\alpha), \quad (4)$$

where q_i denotes the dimensionless normal coordinate for D_i, n is an integer, and $k_{ij\ldots k}^{T-V}$ is a constant. q_i is related to the normal coordinate Q_i by $q_i = 2\pi\sqrt{\frac{\nu_i}{h}}\, Q_i$ (here ν_i is the vibrational frequency and h is Planck's constant) and is used so that the $k_{ij\ldots k}^{T-V}$ can be expressed in units of wavenumber.[50] The number of q terms depends on the changes in vibrational quanta between the states involved in the coupling and defines the order of the coupling term. The total wavefunction is considered a product of torsional and vibrational wavefunctions; the q_i terms operate on the vibrational wavefunction, while the cosine or sine term operates on the torsional wavefunction. Allowed torsion-vibration coupling terms must be totally symmetric (a_1' in G_{12}), which leads to the symmetry constraints on the coupling terms shown in Table III. This table also shows the coupling matrix elements for first order coupling, i.e., a single q term. For these first order terms, we write $k_i^{T-V}\frac{1}{2\sqrt{2}}$ as $V_{T-V}^{(i)}$ and refer to it as the torsion-vibration coupling constant or torsion-vibration coupling matrix element. The higher order torsion-vibration terms similarly have the numerical constants and k^{T-V} combined to form the reported coupling constant.

The torsion-vibration Hamiltonian matrix is constructed for the hindered rotor using a basis of free rotor states to describe the methyl torsion and Harmonic oscillator states

TABLE III. Allowed torsion-vibration coupling terms for molecules of G_{12} symmetry.

Torsion term	Torsion term symmetry	Δm	Vibrational symmetry[a]	Coupling matrix element for first order coupling[b]
$\cos(3\alpha)$	a_1''	± 3	a_1''	$V_{T-V}^{(i)}\upsilon^{\frac{1}{2}}$
$\sin(3\alpha)$	a_2''	± 3	a_2''	$\mp i\, V_{T-V}^{(i)}\upsilon^{\frac{1}{2}}$
$\cos(6\alpha)$	a_1'	± 6	a_1'	$V_{T-V}^{(i)}\upsilon^{\frac{1}{2}}$
$\sin(6\alpha)$	a_2'	± 6	a_2'	$\mp i\, V_{T-V}^{(i)}\upsilon^{\frac{1}{2}}$

[a]In the case of first order coupling, this is the symmetry of the vibrational mode. For higher order coupling, it is the product symmetry of the vibrational modes involved.
[b]Based on the coupling occurring between states with $\upsilon-1$ and υ vibrational quanta. $i \equiv \sqrt{-1}$. The matrix is Hermitian. $V_{T-V}^{(i)} \equiv k_i^{T-V}\frac{1}{2\sqrt{2}}$ (see the text).

to describe the vibrations, with the matrix elements given by Eqs. (1), (2), and (4) (see also Table III). The eigenvalues of this matrix give the eigenstate energies, while the eigenvectors give the coefficients for the eigenstates expressed as linear combinations of the basis states.

A. Torsion-vibration coupling calculations for S_0

Our previous torsion-vibration coupling calculations for S_0 and S_1 toluene involved a single vibrational mode, M_{20},[13,14] because the set of torsion-vibration states observed only involved M_{20}. (M_{20} is the equivalent mode to D_{20} for monosubstituted benzenes.[51]) For pFT, the data set is far more extensive and multiple torsional states have been seen in combination with the low frequency vibrations D_{20}, D_{19}, D_{30}, and, to a lesser extent, D_{14} (see Table I). Consequently, these data provide an opportunity to explore torsion-vibration coupling for several vibrations. A fit of the observed S_0 torsion-vibration state energies was performed including first order torsion-vibration coupling involving D_{20}, D_{19}, D_{30}, and D_{14}. While significant torsional level shifts have only been observed for D_{20}, subtle effects can be accounted for by including the other interactions in the fit; the uncertainties in the parameters provides an indication of the reliability of the coupling constants determined. A second order coupling between D_{19} and D_{14} was also included since this has been observed to perturb the $19_1 m_4$ and $14_1 m_1$ states. In total, the relative energies of 33 states were fitted to 11 parameters. These parameters represent a minimalist set: no anharmonic terms are included and the (unperturbed) torsional barrier is assumed to be the same for all vibrational states. The results of the fit are shown in Table IV, with the parameters determined given in Table V. The uncertainties given for the parameters correspond to one standard deviation as determined by the least squares fitting algorithm. It can be seen that the fit is excellent, with the standard deviation being 0.12 cm^{-1}, which is well within our estimated experimental uncertainty of ±0.2 cm^{-1}. The vibrational frequencies given in Table V are the unperturbed values; the observed values include the effects of torsion-vibration coupling.

Considering the parameters determined (Table V), we note the following:

(i) The two a_2'' out-of-plane methyl wag vibrations D_{19} and D_{20} both have significant torsion-vibration coupling matrix elements, while the out-of-plane a_2' vibration D_{14}, predominantly a ring motion, has a very small coupling. The values of the torsion-vibration coupling matrix elements for D_{19} and D_{20} appear to be well determined based on the uncertainties for these parameters. The D_{19} coupling is particularly large.

(ii) The a_1'' in-plane methyl wag D_{30} has a modest torsion-vibration coupling matrix element, but its value and that of V_6 are closely correlated, leading to large uncertainties in both.

(iii) V_6 is small and positive but has a large uncertainty [see (ii)].

B. Torsion-vibration coupling calculations for S_1

As for S_0, we have fitted the observed band positions to first order torsion-vibration coupling terms for the four

TABLE IV. A comparison between the experimental S_0 torsion-vibration level energies and those determined from the torsion-vibration coupling model fit (see the text). The parameters determined in the fit are shown in Table V.

State	Experiment	Calculated	Obs. − calc.
m_2	16.3	16.4	−0.1
$m_{3(−)}$	48.1	48.1	0.0
$m_{3(+)}$	50.4	50.2	0.3
m_4	81.6	81.7	0.0
m_5	129.6	129.6	0.1
$20_1 m_1$	144.4	144.3	0.0
$20_1 m_2$	162.0	162.0	0.1
$20_1 m_{3(−)}$	183.9	184.2	−0.2
$20_1 m_{3(+)}$	186.0	185.9	0.1
$m_{6(+)}$	204.1	204.2	−0.1
$m_{6(−)}$	205.3	205.3	0.0
$20_1 m_4$	221.7	221.6	0.1
m_7	265.8	265.8	0.0
$20_2 m_0$	288.3	288.3	0.1
$20_2 m_1$	288.9	288.8	0.1
$30_1 m_0$	307.6	307.5	0.1
$30_1 m_1$	307.6	307.5	0.1
$30_1 m_2$	324.0	323.9	0.2
$20_1 m_{6(+)}$	349.9	349.9	0.0
$19_1 m_2$	351.6	351.4	0.1
$20_1 m_{6(−)}$	351.6	351.6	0.0
$30_1 m_{3(+)}$	357.4	357.6	−0.2
$19_1 m_{3(−)}$	383.2	383.0	0.2
$19_1 m_{3(+)}$	385.6	385.7	−0.1
$30_1 m_4$	389.1	389.2	−0.1
$14_1 m_1$	413.2	413.1	0.1
$19_1 m_4$	418.1	417.8	0.3
$19_1 20_1 m_0$	479.1	479.1	0.0
$19_1 20_1 m_1$	479.2	479.3	−0.1
$14_1 20_1 m_1$	559.1	559.2	−0.1
$14_1 m_{6(−)}$	618.8	618.8	−0.1
$19_2 m_0$	670.0	670.1	−0.1
$19_2 m_1$	670.0	670.1	−0.1

vibrations observed and second order coupling terms where such interactions have been observed (see Table II). This involves fitting 30 band positions to 12 parameters. Again,

TABLE V. The parameters determined in the global fits to the S_0 and S_1 torsion-vibration level energies. The values are in units of cm^{-1} and uncertainties correspond to one standard deviation. The vibrational frequencies correspond to unperturbed values.

Parameter	S_0	S_1	
	V_6 varied	V_6 varied	V_6 set to 0
V_6	5.12 ± 2.55	3.69 ± 5.42	0
F	5.516 ± 0.007	5.445 ± 0.023	5.457 ± 0.019
D_{20}	143.17 ± 0.04	104.33 ± 0.15	104.07 ± 0.14
D_{19}	334.19 ± 0.25	239.09 ± 0.39	239.28 ± 0.34
D_{14}	413.53 ± 0.11	198.62 ± 0.18	198.70 ± 0.17
D_{30}	307.35 ± 0.24	308.77 ± 0.91	308.31 ± 0.36
$V_{T-V}^{(20)}$	9.36 ± 0.06	16.12 ± 0.15	16.06 ± 0.15
$V_{T-V}^{(19)}$	21.2 ± 2.7	22.9 ± 1.5	22.3 ± 1.4
$V_{T-V}^{(14)}$	4.1 ± 2.7	0.3 ± 0.9	0.1 ± 0.4
$V_{T-V}^{(30)}$	−7.2 ± 5.8	−7.4 ± 20.4	16.3 ± 3.3
$V_{T-V}^{(14-19)}$	1.24 ± 0.19	2.3 ± 0.3	2.7 ± 0.3
$V_{T-V}^{(20-30)}$	⋯	1.3 ± 1.0	2.6 ± 0.4

these parameters involve a minimalist approach, with the anharmonic terms excluded and the unperturbed torsional barrier assumed to be the same for all vibrational states.

The results of the fit to the S_1 band positions are shown in Table VI, with the parameters determined shown in Table V. The band positions are fitted to a standard deviation of 0.33 cm^{-1}, close to the experimental uncertainty. As noted above, the vibrational frequencies given in Table VI are the unperturbed values. Many of the largest deviations between the calculated and observed values can be traced to the exclusion of anharmonicity from the fit. For example, the calculated 14^1m^1 level is 0.7 cm^{-1} too high in energy, while the calculated 14^2m^1 level is 0.5 cm^{-1} too low. While additional parameters to account for anharmonicity could be added to the fit to improve the calculated band positions, we have not done so since it does not alter the key conclusions, which are as follows:

(i) As was the case for S_0, the two a_2'' out-of-plane methyl wag vibrations, D_{19} and D_{20}, both have large torsion-vibration coupling matrix elements, while the out-of-plane a_2' vibration D_{14}, predominantly a ring motion, has a very small coupling. The coupling matrix

TABLE VI. A comparison between the experimental S_1 torsion-vibration level energies and those determined from the torsion-vibration coupling model fit (see the text). The parameters determined in the fit are shown in Table V.

		V_6 varied		$V_6 = 0$	
State	Observed	Calculated	Obs. – calc.	Calculated	Obs. – calc.
m^2	15.0	15.1	–0.1	15.1	–0.1
$m^{3(-)}$	40.7	40.9	–0.1	40.8	–0.1
$m^{3(+)}$	53.1	52.7	0.4	52.7	0.3
m^4	75.6	75.3	0.3	75.4	0.2
20^1m^2	107.9	107.8	0.1	107.8	0.1
20^1m^1	111.8	111.6	0.2	111.6	0.2
$20^1m^{3(-)}$	137.0	136.7	0.3	136.7	0.3
m^5	140.8	140.8	0.0	140.8	0.0
$20^1m^{3(+)}$	150.1	150.2	–0.1	150.2	–0.1
20^1m^4	172.8	172.9	–0.1	172.9	–0.1
$m^{6(+)}$	196.6	196.6	0.0	196.6	0.0
14^1m^1	197.5	198.3	–0.7	198.2	–0.7
$m^{6(-)}$	201.4	201.4	0.0	201.5	–0.1
20^2m^1	219.3	219.2	0.1	219.2	0.1
20^2m^0	220.1	220.0	0.1	220.0	0.2
19^1m^2	256.6	256.3	0.3	256.3	0.3
m^7	262.1	262.2	0.0	262.1	0.0
$19^1m^{3(-)}$	282.4	282.3	0.1	282.3	0.1
30^1m^1	309.2	308.6	0.5	308.5	0.6
30^1m^0	310.7	310.7	0.1	310.7	0.1
19^1m^4	319.5	319.5	0.0	319.4	0.1
30^1m^2	323.8	324.1	–0.2	324.0	–0.2
$30^1m^{3(-)}$	349.7	350.1	–0.4	350.2	–0.5
$19^120^1m^0$	351.4	352.1	–0.7	352.1	–0.7
$30^1m^{3(+)}$	361.3	361.5	–0.2	361.5	–0.2
30^1m^4	384.5	384.3	0.2	384.5	0.1
14^2m^0	396.9	396.9	0.0	397.0	0.0
14^2m^1	397.3	396.8	0.5	396.7	0.5
19^2m^0	480.3	481.0	–0.7	481.0	–0.7
19^2m^1	482.7	482.0	0.7	482.0	0.6

element for D_{19} is much the same in the two electronic states, but that for D_{20} is substantially larger in S_1.

(ii) Again, as was the case for S_0, the a_1'' in-plane methyl wag D_{30} may have a non-zero torsion-vibration coupling matrix element, but its value and that of V_6 are closely correlated, leading to large uncertainties in both.

(iii) V_6 is small and within the uncertainty of the fit is zero.

A strong correlation between the D_{30} torsion-vibration coupling matrix element and V_6 is seen for both S_0 and S_1 and arises as follows. A correlation between the torsion-vibration coupling terms and V_6 exists because for each vibrational state the torsion-vibration coupling shifts the 3(+) and 3(−) torsional levels, altering their separation, which also depends on V_6 (in the absence of torsion-vibration coupling their separation is $|V_6|/2$). If the coupling constants are well-constrained, V_6 is also then well-constrained to best fit the 3(+)-3(−) separations within each of the vibrations. For D_{19} and D_{20}, the torsion-vibration interactions lead to shifts in many observed states and, consequently, the coupling constants for these two modes are well-constrained. Unfortunately, for D_{30}, the observed bands do not tightly constrain the coupling constant, $V_{T-V}^{(30)}$, and so changes in the 3(+)-3(−) separations arising from changes in $V_{T-V}^{(30)}$ can be compensated by changes in V_6, leading to these two parameters being highly correlated.

The fit for S_1 indicates that V_6 is zero within the uncertainty and, consequently, the "observed" torsional barrier, i.e., twice the $m^{3(-)} - m^{3(+)}$ separation, might be wholly accounted for by the torsion-vibration coupling (see Sec. VI B 1). In view of this, we refitted the data with this parameter set to zero. The resulting fit and parameters are included in Tables V and VI. Setting $V_6 = 0$ leads to little change in the quality of the fit, but as expected it substantially reduces the uncertainty on the torsion-vibration coupling constant for D_{30}, reinforcing that these two parameters are highly correlated.

C. The effect of torsion-vibration coupling on rotational contours

The fits discussed in Secs. V A and V B are based on the torsion-vibration band positions extracted from the images. However, torsion-vibration coupling can also significantly alter the accompanying rotational contours, and this provides another means to assess the accuracy of the torsion-vibration coupling model and the parameters determined by the fits. The reason that the rotational contours can be significantly perturbed by the torsion-vibration coupling is that the rotational states stack up quite differently in the interacting $\underline{m}$ states (which differ by ±3 or ±6) due to the expression for the rotational energy involving an $\underline{m}$ dependence.[11,37,42] The relevant term takes the form $-2A_F'\underline{m}K$, where A_F' is the torsion-rotation coupling constant and K has its usual meaning. In the ideal case of a rigid frame, $A_F' = A_F$, the rotational constant for rotation of the phenyl frame about the a axis,[52] which is ~0.18 cm^{-1} for pFT. Although the torsion-vibration

coupling term, Eq. (4), is independent of the rotational states involved, this $\underline{m}$ dependence of the rotational energy changes the separation between the coupled states and, consequently, changes the amount a state shifts, depending on its K value.

As an illustration, we consider the six features, (m_1^5, m_5^5), $(m_1^5, 20_1^0 m_2^5)$, $(20_0^1 m_0^{3(-)}, 20_1^1 m_{3(-)}^{3(-)})$, $(20_0^1 m_0^{3(-)}, 20_1^1 m_{3(+)}^{3(+)})$, $(20_0^1 m_0^{3(+)} 20_1^1 m_{3(-)}^{3(+)})$, and $(20_0^1 m_0^{3(+)}, 20_1^1 m_{3(+)}^{3(+)})$, seen in Fig. 3. (The first two of these are marked on the figure; the final four are indicated by A, B, C, and D, respectively.) These features are strongly perturbed in S_1 (see Sec. IV B). Furthermore, the two transitions terminating in the S_0 level $20_1 m_{3(+)}$ reveal a rotationally specific perturbation that is manifested by the horizontal features at the bottom left of feature B and the break in the middle of the 2D contour for feature D. Figure 3(b) shows the 2D-LIF image predicted using the parameters determined in the S_0 and S_1 global fits. Comparison with the experimental image, Fig. 3(a), shows that the model calculations accurately capture the rotational contours. Figure 3(c) shows the 2D-LIF image expected for features A–D with no torsion-vibration coupling. The changes in the 2D rotational contours due to the torsion-vibration coupling are obvious when comparing Figs. 3(b) and 3(c). Without torsion-vibration coupling, the experimental rotational structure cannot be reproduced.
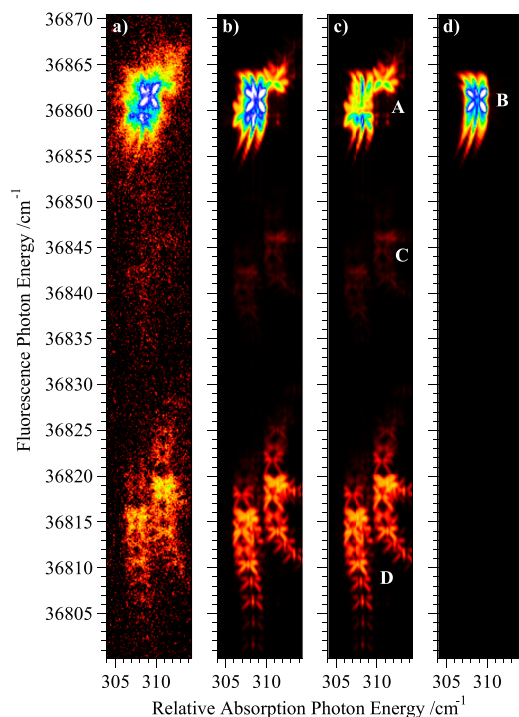
A second example is seen in Fig. 4 which shows how well the complex 2D rotational contours associated with the $30_1 m^0$-$20_1 m^{6(-)}$ interaction are reproduced using the constants determined in the fits to the band positions (Table V).

The accuracy with which the 2D-LIF rotational contours can be predicted, as illustrated by these examples, provides confirmation of the torsion-vibration coupling fits to the torsion-vibration band positions.

VI. DISCUSSION

Figures 5(a) and 5(b) show the observed and predicted S_1 and S_0 states up to 420 and 500 cm^{-1}, respectively, in pFT; those we have observed are shown as solid lines, while those predicted are shown as dashed lines. It can be seen that a reasonable fraction of the states in these regions have been observed. Numerous interactions between the vibrations and methyl torsion have been detected, revealing that torsion-vibration coupling is rife in the lower region of the S_0 and S_1 vibrational manifolds in this molecule.

A. The vibrations observed to interact with methyl torsion

In toluene, the S_0 and S_1 methyl rotor levels are perturbed by a strong torsion-vibration coupling with the out-of-plane methyl wag vibration, M_{20}.[13,14] A key motivation for the present work was to explore the extent to which this type of interaction, which is assumed to be absent in analyses of rotational line data, is also present in pFT. For pFT, we find that there is indeed a significant interaction with the equivalent mode, D_{20}, in both S_0 and S_1. However, the observation of a larger set of states in the case of pFT has revealed that this is not the only mode for which torsion-vibration coupling is significant. D_{19}, which involves an out-of-plane methyl motion similar to that of D_{20}, is also involved in strong coupling with the methyl torsion. By contrast, D_{14}, which involves out-of-plane displacements of ring atoms, couples very weakly with the methyl torsion. These mode dependences to the coupling suggest that methyl group motion during vibration plays a significant role in determining the magnitude of torsion-vibration interaction. In this context, D_{30} would be anticipated to have a strong coupling with the methyl torsion since it involves an in-plane methyl bending motion. Unfortunately, the data are unable to be definitive on this point due to the strong correlation between the value of V_6 and the torsion-vibration coupling constant for D_{30}, although it is interesting to note that for the S_1 $V_6 = 0$ fit, where $V_{T-V}^{(30)}$ has less uncertainty, $V_{T-V}^{(30)}$ is of similar magnitude to $V_{T-V}^{(20)}$.

The torsion-vibration coupling calculations lead to a prediction of the torsion-vibration level structure in the lower manifolds of S_0 and S_1 pFT. Several of the manifolds have quite distorted m state separations as a result of the torsion-vibration coupling. Consideration of the 0_0, 20_1, 20_2, and 20_3 manifolds in S_0, for example, reveals a significant change in the energy separations within the lower m manifold [see Fig. 5(b)]. With the lower D_{20} frequency and stronger torsion-vibration interaction in S_1, the effects are even more striking:
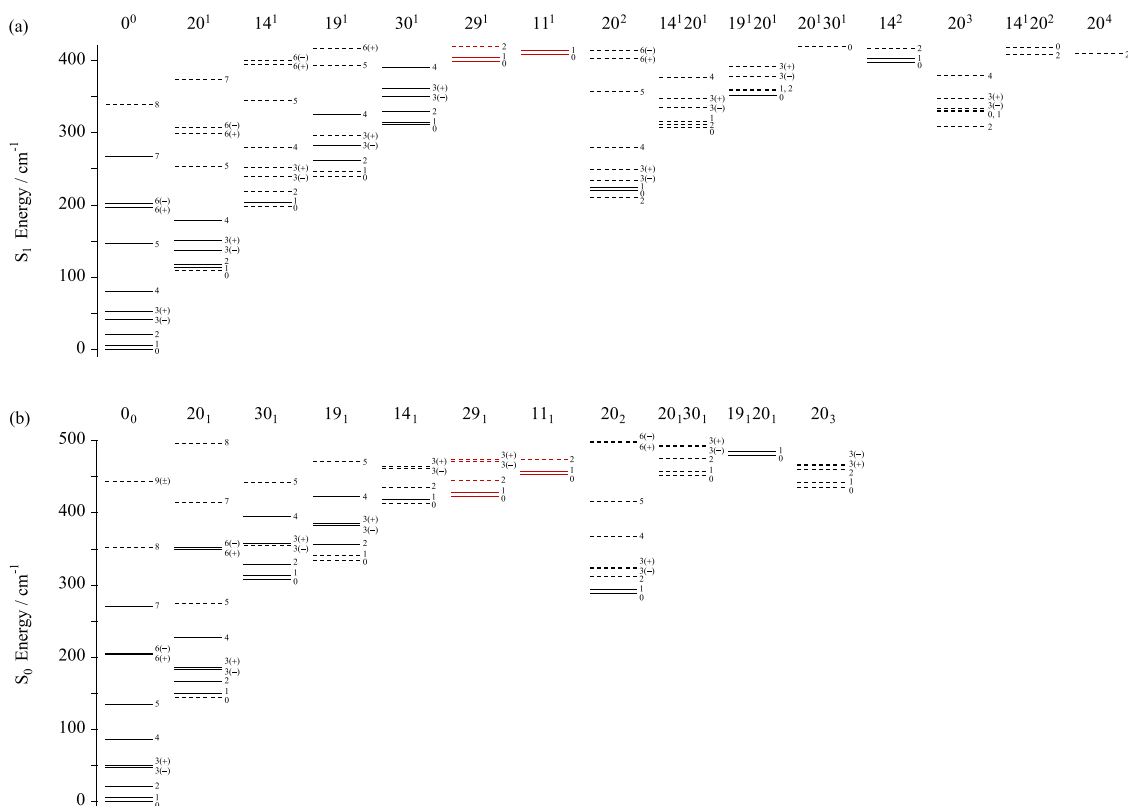

FIG. 4. (a) A 2D-LIF spectral image associated with a scan of the $30_1^1 m_0^0 / 30_1^1 m_1^1$ absorption feature while monitoring emission to $30_1 m_0 / 30_1 m_1$ and $20_1 m_{6(-)}$. The scan reveals emission from $30^1 m^0$ to $20_1 m_{6(-)}$, indicating that the emitting state is of mixed character due to torsion-vibration coupling between $30^1 m^0$ and $20^1 m^{6(-)}$. (b) The image calculated using the parameters derived from the S_0 and S_1 fits with V_6 varied (Table V; see the text). (c) As for (b) but only showing the features associated with excitation from m_0. (d) As for (b) but only showing the features associated with excitation from m_1. The indicated features are (A) $(30_0^1 m_0^0, 30_1^1 m_0^0)$, (B) $(30_0^1 m_1^1, 30_1^1 m_1^1)$, (C) $(30_0^1 m_0^0, 20_2^0 30_0^1 m_{3(+)}^0)$, and (D) $(30_0^1 m_0^0, 20_1^0 30_0^1 m_{6(-)}^0)$.

FIG. 5. (a) The S_1 states up to 420 cm^{-1} and their energies calculated using the constants determined in the fit with V_6 varied (Table V). The states observed are shown as solid lines, while those predicted are shown as dashed lines. The states shown in red were not included in the fit, and where their m states have not been observed, the energies shown are based on the 0^0 torsional energies. (b) As for (a), showing the S_0 states up to 500 cm^{-1}.

for the 20^2 and 20^3 vibrational levels, the m states are predicted to not stack sequentially [see Fig. 5(a)]. A subtle effect is the reversal of the energy ordering of the $m = 6(-)$ and $6(+)$ states in both S_0 and S_1. When calculating the torsional states based solely on a 6-fold torsional barrier, the $m = 6(-)$ state lies below $6(+)$, but a consequence of the torsion-vibration coupling is that $m = 6(-)$ lies above $6(+)$ in both electronic states.

The strongly interacting modes in *p*FT and in S_0 and S_1 toluene[13,14] are those involving an out-of-plane methyl wagging motion. Low frequency modes involving this type of motion will be present in all ring-substituted toluenes. This suggests that for these molecules the widely used assumption that torsion-rotation states can be understood with the small amplitude modes ignored and the problem treated purely in terms of torsion-rotation interactions should be applied with caution.[6,9,11,12,31]

B. Effect of torsion-vibration coupling on molecular constants

The constants extracted from spectroscopic analyses provide important indicators of molecular structures and behaviour, and thus, it is important to have clarity about the constants and their meaning. The presence of torsion-vibration coupling and its explicit incorporation in the spectroscopic analysis lead to values for key constants, most notably V_6 and F, which differ from those determined when torsion-vibration coupling is not explicitly accounted for, as discussed

previously.[12–14] Formulae relating the changes in these values with the torsion-vibration coupling constant have been given previously.[12–14] Here we discuss the changes in key constants due to the torsion-vibration interactions determined for S_0 and S_1 *p*FT.

1. The experimentally determined torsional barrier, V_6

Our fit indicates that the value of V_6 in S_1 is almost zero. In the absence of torsion-vibration coupling, the $3(-)$-$3(+)$ separation of 12.3 cm^{-1} is $|V_6|/2$, which would imply a V_6 value of -24.6 cm^{-1}. The negative value follows because $3(-)$ is observed to lie below $3(+)$, which is associated with a staggered minimum energy configuration.[53] This compares with a value of -33 cm^{-1} reported by Zhao *et al.*[30] However, in our fits, the $3(-)$ and $3(+)$ energies are shifted by the various torsion-vibration couplings and their observed separation no longer indicates the value of V_6. Instead, the observed $3(-)$-$3(+)$ separation is wholly accounted for in S_1 by the torsion-vibration interactions. This illustrates that caution is required when assessing any V_6 value deduced simply from the $3(-)$-$3(+)$ band separations.

The S_0 situation is similar to S_1, but the case for V_6 being accounted for wholly from the interaction of torsion and vibration is not quite as compelling, with the V_6 value determined in the fit being two standard deviations from zero. Both the S_1 and S_0 analyses have, of course, omitted higher lying vibrations that could have an influence on V_6 if they interact strongly with torsion, although with increasing vibrational frequency

the effect is reduced by the increased energy gap between the interacting states.

These considerations lead to the intriguing question of the role of vibrational versus electronic influences on the torsional barrier. The V_6 value associated with our fits pertains to a rigid G_{12} geometry, with the C_3 axis of the methyl lying on the *a*-axis of the frame; the effects of vibration are accounted for through the torsion-vibration coupling terms, and it is these terms that are producing the apparent V_6. This question of the influence of in-plane and out-of-plane vibrations on V_6 was discussed by Walker *et al.* in relation to their *ab initio*-determined "vibrationally adiabatic" torsional potentials.[54] They showed that in a G_{12} molecule the in-plane and out-of-plane vibrational motions create a V_6 component to the torsional potential when the energy, and hence torsional potential, is computed using an optimised geometry at each torsional angle. Since the geometry changes with torsional angles, this so-called vibrationally adiabatic torsional potential inherently includes an interaction of torsion with atomic displacement, i.e., vibration. *Ab initio* calculations of torsional potentials routinely use this vibrationally adiabatic approach and so implicitly incorporate the aspects of any torsion-vibration interaction. The small geometrical changes in a molecule that occur in response to changes in the methyl torsion angle are often referred to as torsional flexing, and the emergence of V_6 potential terms as an outcome of torsional flexing has also been discussed earlier in the context of the shape of 3-fold potential barriers.[55] The case of methanol is particularly interesting in this context as Kwan and Dennison devised a means to simultaneously analyze a set of isotopic variants that allowed torsional potential terms to be transferred between isotopes without modification by torsional flexing.[56] They found that the V_6 term is zero within the experimental uncertainties, although the analysis of single isotopes produces non-zero V_6 terms when fitted to the usual model where torsional flexing is not explicitly accounted for.

2. The torsional constant, F

The second constant that we expect to be significantly affected by the inclusion of torsion-vibration coupling, F, has previously been reported to be 5.46 cm^{-1} in S_0 and ~4.9 cm^{-1} in S_1.[29] Our analysis gives increased values, as expected,[12–14] of 5.516 ± 0.007 cm^{-1} and 5.445 ± 0.023 cm^{-1} in S_0 and S_1, respectively. As was found for toluene, the differences in the F values between S_0 and S_1 are much reduced when torsion-vibration effects are accounted for, and this has important implications for identifying changes that occur in the methyl geometry on electronic excitation. When torsion-vibration coupling is not accounted for, the F values obtained have led to the conclusion that there is a significant change in geometry for the methyl group upon excitation to S_1.[29] However, the inclusion of torsion-vibration coupling leads to the opposite conclusion, i.e., the changes in methyl geometry are small. The changes can be quantified by noting that for *p*FT the methyl C_3 axis lies along the *a* rotational axis for the molecular frame to which it is attached, and in this case, F_α, the rotational constant associated with rotation of the CH_3 group independent of the frame, is related to F by $F_\alpha = F - A_F$, where A_F is the A rotational constant for the frame. A_F for

S_0 *p*FT is 0.190 23 cm^{-1} (Ref. [36]), while the S_1 value is 0.179 cm^{-1} (Ref. [48]), leading to $F_\alpha(S_0) = 5.326$ cm^{-1} and $F_\alpha(S_1) = 5.277$ cm^{-1}, i.e., a change of <1%. The moment of inertia associated with F_α is $I_\alpha = 2m_H r_{CH}^2 (1 - \cos\theta_{HCH})$, where m_H is the mass of hydrogen, r_{CH} is the CH bond length, and θ_{HCH} is the HCH bond angle.[57] The F_α values indicate that the methyl rotor geometry in *p*FT is close to that of methane ($B = 5.241$ cm^{-1}),[58] from which we deduce that the change in F_α from S_0 to S_1 corresponds to either an increase in the CH bond length of 0.006 Å (0.6%) (assuming no change in θ_{HCH}), an increase in the HCH bond angle of 0.9° (0.8%) (assuming no change in r_{CH}), or changes in both. In comparison, the previously reported values for $F(S_0)$ and $F(S_1)$ imply changes that are ~10× larger.

3. The torsion-rotation interaction constant, A'_F

The torsion-rotation Hamiltonian includes a coupling term between the internal rotation (torsion) and overall rotation of the molecule of the form $-2A'_F \underline{m} K$,[11,37,42] where for a rigid molecule the torsion-rotation coupling constant $A'_F = A_F$, the rotational constant for rotation of the phenyl frame about the *a* axis.[52] We predict that as a consequence of the torsion-vibration coupling observed, A'_F will be reduced compared with A_F.[12–14] While there have been no rotational analyses of the torsional states in S_1, Ghosh has reported the results of an analysis of the microwave spectrum for the S_0 torsional levels.[35] He reports $A_F = 5702.373$ MHz and $A'_F = 5660.16$ MHz, 5658.215 MHz, and 5657.767 MHz for $m = 1, 2,$ and 4, respectively. These A'_F values are considerably less than A_F as expected. We have presented perturbation-based expressions for the effect of torsion-vibration coupling on A'_F previously.[12] In the present case, there are two strongly interacting modes, D_{19} and D_{20}. Substituting the constants determined in our fit (Table V) into the perturbation-based expressions predicts values for A'_F for $m = 1, 2,$ and 4 of 5654 MHz, 5647 MHz, and 5580 MHz, respectively. While the $m = 1$ and 2 values are reasonably close to those reported by Ghosh, the $m = 4$ value is significantly lower. This predicted decrease is caused by a strong interaction between the states m_4 and $20_1 m_1$, as their separation is only 63 cm^{-1}. Ghosh has noted that the change in A'_F with m in his fits is small, and he comments that this "arises partly from a correlation with other constants which change with *m*."[35] Consequently, it may be that the larger change in A'_F that we predict for $m = 4$ is masked by this effect. A reappraisal of the microwave spectrum of *p*FT would be useful to explore this issue.

C. Implications for IVR

The observation of strong torsion-vibration coupling in *p*FT involving multiple low frequency vibrational modes together with a number of second order couplings has implications for intramolecular vibrational energy redistribution (IVR). As noted in the Introduction, the presence of a methyl rotor was identified early as an accelerator for IVR in excited aromatics, with S_1 *p*FT being the textbook example.[16–21] The classical Hamiltonian modeling of Martens and Reinhardt of the S_1 vibrations of *p*FT found that the methyl rotor and the lowest-frequency modes interact strongly and chaotically,

leading to rapid energy exchange amongst them, which is consistent with our observation of strong coupling involving D_{19} and D_{20}.[32] More recent examples of the influence of torsion have been seen in time resolved photoelectron spectra, following excitation near 800 cm^{-1} and 2000 cm^{-1} in S$_1$.[59–61] Interestingly in the context of torsion-vibration interaction, Davies *et al.*[61] modeled the mode dependence observed near 2000 cm^{-1} using a van der Waals based torsion-vibration interaction as proposed by Moss *et al.*[17] (*vide infra*). Recently, Gardner *et al.* have used 2D-LIF to illuminate torsion-vibration interactions involving S$_1$ states near 850 cm^{-1},[28] a region also probed previously using time resolved photoelectron spectroscopy.[60] Tuttle *et al.* have discussed the key aspects of IVR based on a series of related molecules: *p*-difluorobenzene, *p*-chlorofluorobenzene, *p*FT, and *p*-xylene.[62] In the context of the effects of a methyl rotor, they conclude that its addition opens up new routes for coupling vibrations of different symmetry. They also note the role of serendipity in energy resonances leading to strong mixing. Our observation of torsion-vibration coupling involving multiple low frequency modes provides further experimental confirmation that torsion-vibration interactions are operating in *p*FT. We note that the presence of torsion-vibration coupling does not exclude the possibility of contributions to the methyl rotor's enhancement of IVR from other mechanisms, such as the electronic interaction proposed by Borst and Pratt.[42]

Moss *et al.* proposed a torsion-vibration coupling mechanism to explain the origin of the methyl rotor enhancement of IVR and presented a model for *p*FT based on intramolecular van der Waals interactions as the underlying mechanism responsible for this coupling.[17] These authors predicted torsion-vibration coupling constants for several low frequency modes of different symmetry in S$_1$ *p*FT, but there have been no experimental values against which to compare these predictions. They calculate V_{T-V} = 7.9 cm^{-1} for D_{20}, which is ~50% of the value we have determined in our analysis of the spectrum. They suggested the empirical formula $V \approx 0.3^{|\Delta v|-1} \times 4$ cm^{-1}, where Δv is the total number of vibrational quanta difference between the coupled states, which yields first order and second order coupling terms of 4 and 1.2 cm^{-1}, respectively. Our analysis of S$_1$ indicates that this underestimates the magnitude of the first order couplings for D_{19} and D_{20} but is quite close to the second order terms observed.

An important corollary of the involvement of the lowest frequency modes in torsion-vibration coupling is that all vibrational states will be mixed by the interaction to some extent, since a generic state $X\ m^n$ couples to $X\ 20^1\ m^{n\pm3}$ and $X\ 19^1$ $m^{n\pm3}$. Such coupling is weakest for the low n case due to the large energy separation of the coupled states. This perhaps explains the observations of Davies *et al.*, who used time-resolved photoelectron spectroscopy to examine IVR from an equivalent vibrational level in toluene, toluene-d_3, and *p*FT at ~1200 cm^{-1} and concluded that, at least for this level, the presence of doorway states is more important than coupling pathways involving torsional modes.[63] As a result of the low frequencies of D_{19} and D_{20}, the density of states will be dominated by overtones and combination bands involving them, thereby providing a coupling network via torsion-vibration interactions. The involvement of the low frequency modes

in promoting state mixing via this mechanism means that it will be extensive amongst the background states at higher energy. Weaker second order couplings also appear to be operating, which would further enhance the state mixing that is an essential precursor to IVR.

VII. CONCLUSIONS

We have reported 2D-LIF images exploring the lower torsion-vibration manifold in S$_0$ ($E < 560$ cm^{-1}) and S$_1$ ($E < 420$ cm^{-1}) *p*FT. This work has provided a definitive set of assignments for the low frequency regions in S$_0$ and S$_1$ *p*FT, the latter confirming the recent revised assignments of Gardner *et al.*[26] and, by extension, their assignments for the ground state of the cation, D_0^+. Unequivocal spectral evidence has been provided for a number of first and second order torsion-vibration interactions.

Modeling of the band positions reveals that the two lowest frequency, out-of-plane methyl wag vibrations, D_{19} and D_{20}, couple strongly to the methyl torsion (internal rotation) in both S$_0$ and S$_1$. By contrast, the low frequency out-of-plane ring mode D_{14} couples only weakly, suggesting that methyl motion may be important in the torsion-vibration interaction. The evidence for torsion-vibration coupling involving the in-plane methyl wag mode, D_{30}, is inconclusive due to a strong correlation between the torsion-vibration coupling constant for this mode and the torsional barrier height, V_6. *p*FT is the second aromatic, following toluene,[12–14] for which a strong coupling between torsion and methyl out-of-plane wagging vibrations has been identified and quantified. All substituted toluenes will have one or more vibrational modes involving the equivalent methyl wagging motion, and thus, this mechanism for torsion-vibration coupling may be widespread in these types of molecules, including those with, for example, nitrogen substituted in the ring. Clearly, there is a need for such molecules to be explored to determine how pervasive these types of torsion-vibration interactions are. As demonstrated previously for toluene[12–14] and now for *p*FT, when torsion-vibration coupling is explicitly included in the analysis, key molecular constants such as torsional barrier heights and torsional (and rotational) constants are affected. Consequently, we suggest that the possibility for torsion-vibration coupling should be considered in spectral analyses of these types of molecules.

The observation of strong torsion-vibration coupling has implications for intramolecular vibrational energy redistribution (IVR) in *p*FT. The involvement of the low frequency modes in promoting state mixing via this mechanism means that it will be pervasive in overtones and combination bands at higher energy. Weaker second order couplings also appear to be present. These observations are consistent with torsion-vibration coupling contributing to the enhanced IVR observed in this molecule compared with *p*-difluorobenzene, as proposed by Moss *et al.*[17]

SUPPLEMENTARY MATERIAL

See supplementary material for a detailed description of the analysis and assignment of the spectral features seen

in the 2D-LIF images and the torsion-vibration interactions revealed.

[1] D. G. Lister, J. N. Macdonald, and N. L. Owen, *Internal Rotation and Inversion: An Introduction to Large Amplitude Motions in Molecules* (Academic Press, London, 1978).

[2] J. D. Kemp and S. P. Kenneth, J. Chem. Phys. **4**, 749 (1936).

[3] V. Pophristic and L. Goodman, Nature **411**, 565 (2001).

[4] Y. Mo and J. Gao, Acc. Chem. Res. **40**, 113 (2007).

[5] F. Cortés-Guzmán, G. Cuevas, Á. M. Pendás, and J. Hernández-Trujillo, Phys. Chem. Chem. Phys. **17**, 019021 (2015).

[6] I. Kleiner, J. Mol. Spectrosc. **260**, 1 (2010).

[7] P. Groner, J. Mol. Spectrosc. **278**, 52 (2012).

[8] See http://www.ifpan.edu.pl/~kisiel/prospe.htm for PROSE: Programs for ROtational SPEctroscopy.

[9] V. V. Ilyushin, Z. Kisiel, L. Pszczólkowski, H. Mäder, and J. T. Hougen, J. Mol. Spectrosc. **259**, 26 (2010).

[10] E. B. Wilson, Jr., C. C. Lin, and D. R. Lide, Jr., J. Chem. Phys. **23**, 136 (1955).

[11] W. Gordy and R. L. Cook, *Microwave Molecular Spectra* (Wiley New York, 1970), see Chap. 12.

[12] J. R. Gascooke and W. D. Lawrance, J. Mol. Spectrosc. **318**, 53 (2015).

[13] J. R. Gascooke, E. A. Virgo, and W. D. Lawrance, J. Chem. Phys. **142**, 024315 (2015).

[14] J. R. Gascooke, E. A. Virgo, and W. D. Lawrance, J. Chem. Phys. **143**, 044313 (2015).

[15] J. R. Gascooke and W. D. Lawrance, Eur. Phys. J. D **71**, 287 (2017).

[16] C. S. Parmenter and B. M. Stone, J. Chem. Phys. **84**, 4710 (1986).

[17] D. B. Moss, C. S. Parmenter, and G. E. Ewing, J. Chem. Phys. **86**, 51 (1987).

[18] Q. Ju, C. S. Parmenter, T. A. Stone, and Z. Q. Zhao, Isr. J. Chem. **37**, 379 (1997).

[19] R. J. Longfellow and C. S. Parmenter, J. Chem. Soc., Faraday Trans. 2 **84**, 1499 (1988).

[20] D. B. Moss and C. S. Parmenter, J. Chem. Phys. **98**, 6897 (1993).

[21] P. J. Timbers, C. S. Parmenter, and D. B. Moss, J. Chem. Phys. **100**, 1028 (1994).

[22] A. M. Gardner, A. M. Green, V. M. Tamé-Reyes, V. H. K. Wilton, and T. G. Wright, J. Chem. Phys. **138**, 134303 (2013).

[23] A. M. Gardner, A. M. Green, V. M. Tamé-Reyes, K. L. Reid, J. A. Davies, V. H. K. Parkes, and T. G. Wright, J. Chem. Phys. **140**, 114308 (2014).

[24] W. D. Tuttle, A. M. Gardner, K. B. O'Regan, W. Malewicz, and T. G. Wright, J. Chem. Phys. **146**, 124309 (2017).

[25] A. M. Gardner, W. D. Tuttle, P. Groner, and T. G. Wright, J. Chem. Phys. **146**, 124308 (2017).

[26] A. M. Gardner, W. D. Tuttle, L. Whalley, A. Claydon, J. H. Carter, and T. G. Wright, J. Chem. Phys. **145**, 124307 (2016).

[27] W. D. Tuttle, A. M. Gardner, L. E. Whalley, and T. G. Wright, J. Chem. Phys. **146**, 244310 (2017).

[28] A. M. Gardner, W. D. Tuttle, L. E. Whalley, and T. G. Wright, Chem. Sci. **9**, 2270 (2018).

[29] K. Okuyama, N. Mikami, and M. Ito, J. Phys. Chem. **89**, 5617 (1985).

[30] Z. Q. Zhao, C. S. Parmenter, D. B. Moss, A. J. Bradley, A. E. W. Knight, and K. G. Owens, J. Chem. Phys. **96**, 6362 (1992).

[31] K. P. R. Nair, M. K. Jahn, A. Lesarri, V. V. Ilyushin, and J.-U. Grabow, Phys. Chem. Chem. Phys. **17**, 26463 (2015).

[32] C. C. Martens and W. P. Reinhardt, J. Chem. Phys. **93**, 5621 (1990).

[33] J. R. Gascooke, U. N. Alexander, and W. D. Lawrance, J. Chem. Phys. **134**, 184301 (2011).

[34] J. R. Gascooke and W. D. Lawrance, J. Chem. Phys. **138**, 134302 (2013).

[35] P. N. Ghosh, J. Mol. Spectrosc. **138**, 505 (1989).

[36] J. Rottstegge, H. Hartwig, and H. Dreizler, J. Mol. Struct. **478**, 37 (1999).

[37] E. A. Virgo, J. R. Gascooke, and W. D. Lawrance, J. Chem. Phys. **140**, 154310 (2014).

[38] L. H. Spangler, Annu. Rev. Phys. Chem. **48**, 481 (1997).

[39] K. T. Lu, G. C. Eiden, and J. C. Weisshaar, J. Phys. Chem. **96**, 9742 (1992).

[40] K. T. Lu and J. C. Weisshaar, J. Chem. Phys. **99**, 4247 (1993).

[41] L.-H. Xu, J. Fisher, R. M. Lees, H. Y. Shi, J. T. Hougen, J. C. Pearson, B. J. Drouin, G. A. Blake, and R. Braakman, J. Mol. Spectrosc. **251**, 305 (2008).

[42] D. R. Borst and D. W. Pratt, J. Chem. Phys. **113**, 3658 (2000).

[43] P. J. Breen, J. A. Warren, E. R. Bernstein, and J. I. Seeman, J. Chem. Phys. **87**, 1917 (1987).

[44] R. A. Walker, E. Richard, K. T. Lu, E. L. Sibert, and J. C. Weisshaar, J. Chem. Phys. **102**, 8718 (1995).

[45] A. Andrejeva, A. M. Gardner, W. D. Tuttle, and T. G. Wright, J. Mol. Spectrosc. **321**, 28 (2016).

[46] J. H. S. Green, Spectrochim. Acta, A **26**, 1503 (1970).

[47] D. W. Scott, J. F. Messerly, S. S. Todd, I. A. Hossenlopp, D. R. Douslin, and J. P. McCullough, J. Chem. Phys. **37**, 867 (1962).

[48] T. Cvitaš and J. M. Hollas, Mol. Phys. **20**, 645 (1971).

[49] E. C. Richard, R. A. Walker, and J. C. Weisshaar, J. Chem. Phys. **104**, 4451 (1996).

[50] E. B. Wilson, J. C. Decius, and P. C. Cross, *Molecular Vibrations: The Theory of Infrared and Raman Vibrational Spectra* (Dover Publications, Inc., New York, 1955).

[51] A. M. Gardner and T. G. Wright, J. Chem. Phys. **135**, 114305 (2011).

[52] K. Mitra and P. N. Ghosh, J. Mol. Spectrosc. **109**, 374 (1985).

[53] R. D. Gordon and J. M. Hollas, Chem. Phys. Lett. **164**, 255 (1989).

[54] R. A. Walker, E. C. Richard, K.-T. Lu, and J. C. Weisshaar, J. Phys. Chem. **99**, 012422 (1995).

[55] R. M. Lees, J. Chem. Phys. **59**, 2690 (1973), and references therein.

[56] Y. Y. Kwan and D. M. Dennison, J. Mol. Spectrosc. **43**, 291 (1972).

[57] C. H. Townes and A. L. Schawlow, *Microwave Spectroscopy* (McGraw-Hill, New York, 1955).

[58] G. Herzberg, *Molecular Spectra and Molecular Structure. III. Electronic Spectra of Polyatomic Molecules* (Van Nostrand, New York, 1966).

[59] J. A. Davies and K. L. Reid, Phys. Rev. Lett. **109**, 193004 (2012).

[60] J. A. Davies and K. L. Reid, J. Chem. Phys. **135**, 124305 (2011).

[61] J. A. Davies, L. E. Whalley, and K. L. Reid, Phys. Chem. Chem. Phys. **19**, 5051 (2017).

[62] W. D. Tuttle, A. M. Gardner, L. E. Whalley, D. J. Kemp, and T. G. Wright, "Effects of symmetry, methyl groups and serendipity on intramolecular vibrational energy dispersal," Phys. Chem. Chem. Phys. (in press).

[63] J. A. Davies, A. M. Green, A. M. Gardner, C. D. Withers, T. G. Wright, and K. L. Reid, Phys. Chem. Chem. Phys. **16**, 430 (2014).